Polarimetric Radar Estimators Based on a Constrained Gamma Drop Size Distribution Model

J. VIVEKANANDAN, GUIFU ZHANG, AND EDWARD BRANDES

National Center for Atmospheric Research, Boulder, Colorado

(Manuscript received 16 September 2002, in final form 24 July 2003)

ABSTRACT

Raindrop size distribution (DSD) retrieval from remote radar measurements or from in situ disdrometer measurements is an important area of research. If the shape (μ) and slope (Λ) of a three-parameter gamma distribution $n(D) = N_0 D^{\mu} \exp(-\Lambda D)$ are related to one another, as recent disdrometer measurements suggest, the gamma DSD model is simplified to a two-parameter DSD, that is, a constrained gamma DSD. An empirical relation between the μ and Λ was derived using moments estimated from video-disdrometer measurements. Here, the effects of DSD truncation on a μ and Λ relation were analyzed. It was shown that characteristic size and variance of size of a constrained gamma DSD depend only on the shape parameter μ. Assuming that a constrained gamma DSD is valid, S-band polarimetric radar–based estimators for rain rate, median volume diameter, specific propagation phase, attenuation, and differential attenuation were derived. The radar-based estimators were used to obtain the spatial distribution of DSD parameters corresponding to a range–height indicator of radar measurements. Self-consistency among polarization radar measurements is used to indirectly verify constrained gamma DSD-based polarization radar estimators.

1. Introduction

One of the factors that limits accuracy of rain-rate estimation by a well-calibrated radar is a lack of detailed knowledge of drop size distribution (DSD). Rain rate R is usually estimated from radar reflectivity Z using a $Z(R)$ relation based on convective or stratiform rain. The $Z(R)$ relation was obtained by regression analysis of gauge measurements and radar reflectivity. It is known that the $Z(R)$ relation changes from each location and time, depending on changes in the DSD. Therefore, a fixed empirical $Z(R)$ relation cannot provide accurate rain estimation for various types of rain because it cannot represent variations in rain DSD. The relation between radar reflectivity and rain rate is almost completely quantified only if the drop size distribution is specified because they are proportional to moments of DSD; namely, S-band reflectivity is approximately the sixth moment and rain rate is proportional to the 3.67th moment of the drop spectrum. Accurate rain-rate estimation requires detailed knowledge of the rain DSD and, hence, various rain-rate estimators are derived using polarimetric radar observations that include reflectivity, differential reflectivity, and propagation phase (Doviak and Zrnic 1993).

The polarimetric radar technique has attracted great attention because most of the hydrometeors are nonspherical. Particularly in the case of raindrops there is a well-defined relation between characteristic size D and shape (Seliga and Bringi 1976; Oguchi 1983). The polarization radar measurements provide additional information about precipitation and allow better microphysical characterization of hydrometeors (Vivekanandan et al. 1999a). In general, Z, differential reflectivity (Z_{DR}), and specific propagation phase (K_{DP}) are used for estimating rain rate and drop spectrum, because they depend mainly on drop size and shape (Jameson 1983). A linear depolarization ratio (LDR) and the cross correlation between co- and cross-polarized radar signals are used for retrieving canting angles because they are sensitive to particle orientation (Ryzhkov et al. 1999; Vivekanandan et al. 1999b).

In some of the earlier studies, rain DSD was assumed to be an exponential distribution with two parameters (N_0, Λ) (Sachidananda and Zrnić 1987). Early rain DSDs (Marshall and Palmer 1948; Laws and Parson 1943) indicate a special case of exponential distribution. The reasons for using exponential distribution are as follows:

1) Two parameters (N_0, Λ) of exponential distribution may be inferred from Z and Z_{DR} or attenuation A (Seliga and Bringi 1976; Ulbrich 1983).
2) This method might be good enough for rain estimation as long as the ''central moments'' are used for estimating exponential distribution (Smith 1998).

Corresponding author address: Dr. J. Vivekanandan, National Center for Atmospheric Research, P.O. Box 3000, Boulder, CO 80307-3000.
E-mail: vivek@ucar.edu

3) Rain DSD, averaged over a long time period, tends to be exponentially distributed (Yuter and Houze 1997).

However, for a standard sampling time, such as 1 min, some observations indicate that natural rain DSD contains fewer of both very large and very small drops than an exponential distribution (Ulbrich 1983; Tokay and Short 1996). Estimated rain rate may be comparable to the actual rain rate of the measured spectrum, using either exponential distribution or a gamma distribution with a fixed μ when the third or fourth moment is included, because rain rate proportional to the 3.67th moment is the closest to moments used for estimating DSD parameters. However, the problem of the assumed exponential or a gamma distribution with a fixed μ distribution would not be able to provide other moments that are much different from the ones used for estimating DSD parameters, such as reflectivity or attenuation, at a radar wavelength comparable to raindrop size.

Ulbrich (1983) suggested the use of the gamma distribution for representing a raindrop spectrum as

$$n(D) = N_0 D^{\mu} \exp(-\Lambda D). \quad (1)$$

Because the three DSD parameters do not correspond to physical parameters, such as liquid water content or median volume diameter, various normalization techniques were used (Willis 1984; Dou et al. 1999). A normalized gamma distribution was first proposed by Willis (1984), and was recently adopted by Illingworth and Blackman (2002) to eliminate the dependence between N_0 and μ (Willis 1984; Chandrasekar and Bringi 1987; Illingworth and Blackman 2002; Testud et al. 2001). They recommend using physically meaningful parameters to characterize a gamma DSD. Nevertheless, the number of DSD parameters remains the same, and the DSD expression becomes more complicated. In practice, there is no simplification of the DSD function except that DSD parameters are expressed using total number concentration, liquid water content, and D_0.

Most of the studies that deal with in situ DSD observation describe methods for obtaining parameters of various mathematical functions to fit the observed discrete DSD. The technique for retrieving DSD parameters from a limited number of radar measurements is an important area of research. More importantly, techniques for retrieving a general DSD function, using the commonly observed radar measurements, are intriguing. Reflectivity and differential reflectivity Z_{DR} are directly measured at every gate, whereas K_{DP} is the range derivative of Φ_{DP}, the differential propagation phase, averaged over a number of gates. Combining gate-by-gate measurements of Z_{HH} and Z_{DR} with the range-smoothed K_{DP} for DSD retrieval causes degradation in spatial resolution. In general, only Z_{HH} and Z_{DR} are used for DSD parameter retrieval in the case of exponential distribution or gamma distribution with fixed μ (Bringi et al. 1998). An additional relation is needed for retrieving the three parameters of the gamma distribution. An N_0–μ relation was used with radar reflectivity and attenuation for retrieving all three parameters of a gamma DSD (Ulbrich 1983).

In this paper, we study constrained gamma rain DSD and its application to rain estimation from polarimetric radar measurements. In section 2 the three parameters of gamma DSD are obtained from three moments of the measured DSD. Measured size distributions are truncated at small- and large-particle limits, depending on the instrumentation limitation. Effects of truncation on size distribution are investigated. In section 3, a constrained relation between μ and Λ is derived from disdrometer observations and is analyzed using truncated and untruncated moments of the drop size spectra. Also, possible physical explanations for μ–Λ are presented. In section 4, various characteristic raindrop sizes are derived as a function of DSD shape. Using constrained gamma DSD, polarization radar–based estimators for rain rate, median drop size, specific propagation phase, attenuation, and differential attenuation are obtained in section 5. Spatial distribution of the raindrop spectrum is shown for a vertical cross section of a rainstorm. A specific propagation phase is obtained from Z and Z_{DR} observations. The estimated propagation phase using Z and Z_{DR} measurements is compared with the actual measured propagation phase for verifying the applicability of constrained gamma DSD polarimetric radar–based relations in section 6. A summary of the results is given in section 7.

2. DSD parameters using untruncated- and truncated-moment methods

Raindrop size distribution can be measured using various instruments, such as a momentum impact disdrometer, a Particle Measuring System (PMS) probe, and video disdrometer (Yuter and Houze 1997; Williams et al. 2000). Both the disdrometer and PMS probe observations are affected by the sampling limitation in measuring small and large drops. Thus, estimations of DSD parameters from these instruments should take into account effects due to truncation on measured discrete drop size spectra. For long sample periods, DSD was commonly assumed to be an exponential, but in situ observation indicates that instantaneous rain DSD is better characterized by a three-parameter gamma distribution $n(D) = N_0 D^{\mu} \exp(-\Lambda D)$. In this study, the video-disdrometer measurements collected in the PRECIP98 field experiment (Brandes et al. 2002) are analyzed. The video disdrometer was operated by the University of Iowa in east-central Florida during the summer of 1998 when the National Center for Atmospheric Research (NCAR)'s S-band dual-polarization Doppler radar (S-Pol) was also deployed to evaluate the potential of polarimetric radar for estimating rain in a tropical environment. Following below is a brief review

of the method of fitting the measured DSDs to a gamma distribution and finding the relations among the DSD parameters.

The moment method is widely accepted in the meteorology community because of its robustness in obtaining parameters of DSD from disdrometer measurements of a spectrum that may not be as well-defined a function as a gamma distribution (Kozu and Nakamura 1991; Tokay and Short 1996; Ulbrich and Atlas 1998). Assuming untruncated DSD, the integration of most moment calculations are usually performed from zero to infinite size range as

$$\langle D^n \rangle = \int_0^\infty D^n n(D)\, dD = N_0 \Lambda^{-(\mu+n+1)} \Gamma(\mu + n + 1). \quad (2)$$

In general, the three parameters (N_0, μ, and Λ) can be solved from any three moments, such as the second, fourth, and sixth. To eliminate Λ and find μ, a ratio is defined as

$$\eta = \frac{\langle D^4 \rangle^2}{\langle D^2 \rangle \langle D^6 \rangle} = \frac{(\mu + 3)(\mu + 4)}{(\mu + 5)(\mu + 6)}. \quad (3)$$

Then, μ can be easily solved from (3) as

$$\mu = \frac{(7 - 11\eta) - [(7 - 11\eta)^2 - 4(\eta - 1)(30\eta - 12)]^{1/2}}{2(\eta - 1)}, \quad \text{and} \quad (4)$$

Λ can be calculated from

$$\Lambda = \left[\frac{\langle D^2 \rangle \Gamma(\mu + 5)}{\langle D^4 \rangle \Gamma(\mu + 3)}\right]^{1/2} = \left[\frac{\langle D^2 \rangle (\mu + 4)(\mu + 3)}{\langle D^4 \rangle}\right]^{1/2}. \quad (5)$$

As shown in (2), N_0 can be calculated from any of the three moments for specified μ and Λ.

It should be noted that the integration in (2) is performed from 0 to infinity, that is, an untruncated size distribution. In practice, raindrop distribution is measured over a finite sample volume and time; hence, only a finite number of raindrops were observed within a finite size range ($D_{\min}$, $D_{\max}$) because of practical and sampling limitation in measuring small and large drops. The typical range of raindrop size estimated by the Joss disdrometer is between 0.3 and 5 mm, while a video disdrometer can measure raindrop size between 0.1 and 8 mm. However, the above-described method for estimating DSD parameters is applicable only for untruncated DSD. For a gamma distribution with a truncated size range, the statistical moments are calculated as

$$\langle D^n \rangle = \int_{D_{\min}}^{D_{\max}} D^n n(D)\, dD = N_0 \Lambda^{-(\mu+n+1)} [\gamma(\mu + n + 1, \Lambda D_{\max}) - \gamma(\mu + n + 1, \Lambda D_{\min})], \quad (6)$$

where $\gamma(\ldots)$ is an incomplete gamma function. As expected, the truncated moments depend on the upper and lower limits of droplet size in the measured spectrum. If the moments obtained from (6) are used to fit a truncated gamma distribution, using the above untruncated-moment method described in Eqs. (2)–(5), the resultant DSD parameters may be in error.

Figure 1 shows three gamma distributions with a fixed liquid water content (LWC) of 1 g m^{-3} and a median volume diameter D_0 of 1.5 mm. For a specific set of LWC and D_0, the parameter μ (or Λ) can be freely chosen based on a $\Lambda D_0 = 3.67 + \mu$ relation. When μ is 0.0, 2.0, or 4.0, then Λ and N_0 can be calculated accordingly. Using the above-described truncated-moment method, DSD parameters can be estimated as a function of lower and upper bounds of the drop size spectrum. Figures 2 and 3 show retrieved DSD parameters as a function of the lower limit $D_{\min}$ and upper limit $D_{\max}$ of the spectrum. All three DSD parameters N_0, μ, and Λ increase as the spectrum is truncated (increase in $D_{\min}$ or decrease in $D_{\max}$), that is, as the spectrum becomes narrower. Thus, use of truncated moments instead of untruncated moments in Eqs. (3), (4), and (5) introduces significant error in the estimated DSD parameters. The potential for error is larger for a spectrum

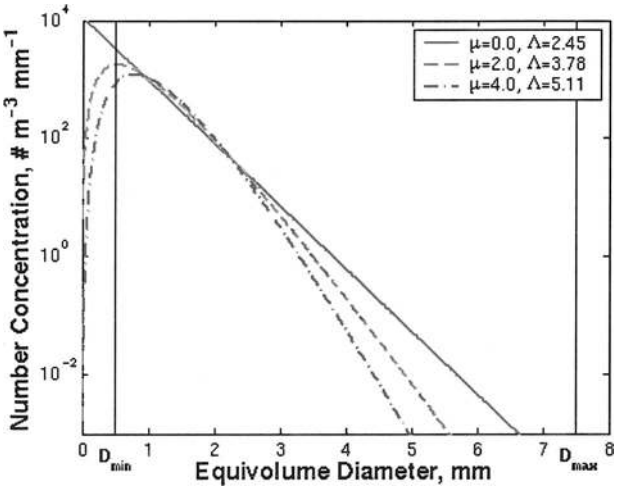

FIG. 1. Gamma distributions for fixed liquid water content of 1 g m^{-3} and median volume diameter of 1.5 mm. Parameter μ (or Λ) can be freely chosen based on the $\Lambda D_0 = 3.67 + \mu$ relation.

with small values of μ and Λ. It can be inferred from Figs. 2 and 3, that as long as $D_{\min} < 0.5\ D_0$ and $D_{\max} > 4\ D_0$ are satisfied, the effect of truncation on retrieved parameters is less than 5%.

Overestimating DSD parameters can be minimized when appropriate truncated moments are used. Using the truncated moments shown in Eq. (6), moments consistent with truncation can be calculated, and then the corresponding expressions for DSD parameters can be derived as follows:

$$\eta = \frac{[\gamma(\mu + 5, \Lambda D_{\max}) - \gamma(\mu + 5, \Lambda D_{\min})]^2}{\gamma(\mu + 3, \Lambda D_{\max})\gamma(\mu + 7, \Lambda D_{\max}) - \gamma(\mu + 3, \Lambda D_{\min})\gamma(\mu + 7, \Lambda D_{\min})}, \quad \text{and} \tag{7}$$

$$\Lambda = \left\{\frac{\langle D^2\rangle[\gamma(\mu + 5, \Lambda D_{\max}) - \gamma(\mu + 5, \Lambda D_{\min})]}{\langle D^4\rangle[\gamma(\mu + 3, \Lambda D_{\max}) - \gamma(\mu + 3, \Lambda D_{\min})]}\right\}^{1/2}. \tag{8}$$

Equations (7) and (8) constitute joint equations for μ and Λ for the truncated moments that are difficult to separate from each other. Because the above equations are nonlinear, an iterative approach is necessary for solving μ and Λ as follows: (i) estimate initial value of μ and Λ from Eqs. (3)–(5), (ii) calculate η from (7) and compare it with the actual measured-moment ratio, and (iii) if the moment-two ratios are different, μ and Λ are adjusted using (8) until η from (7) converges to the actual measured-moment ratio.

3. Analysis of the μ–Λ relation

Video-disdrometer measurements collected in PRECIP98 are used in this study. The dataset is the same as that reported in Zhang et al. (2001), except minor revisions were made for splashing and wind effects during DSD measurements. We use the untruncated- and truncated-moment methods to fit the measured DSDs with a gamma distribution.

Figure 4 shows an example of measured rain DSD and gamma distribution fit. The solid line uses the moment method, and the dashed line the truncated-moment method. Visually, both truncated- and untruncated-moment-based DSD parameters fit the measurement well, and they give a consistent rain-rate and drop size estimation. The rain rate from the measured DSD is 74.9 mm h^{-1} and the calculated rain rate from the untruncated-moment method is 79.6 mm h^{-1}, which from truncated moments is 79.2 mm h^{-1}. The median volume diameter D_0 is 2.35 and 2.43 mm, respectively, when untruncated and truncated moments are used. The gamma DSD parameters, however, are different for untruncated and truncated methods, and corresponding values of N_0, μ, and Λ are (7332, 0.67, 1.85) and (5441, 0.031, 1.53), respectively. Even though truncated- and untruncated-moment methods produce similar rain rate and D_0, the corresponding DSD parameters are different.

Figure 5 shows the scatterplots of the fitted DSD parameters (μ versus Λ). Figure 5a is obtained from the untruncated-moment method and Fig. 5b is from the truncated-moment method. There are a total of 1341 1-min DSD spectra, covering over 22 h in 17 days during PRECIP98 (Brandes et al. 2001). Both Figs. 5a and 5b show correlation between μ and Λ. However, retrievals of μ and Λ obtained using the truncated-moment method show better correlation than the corresponding set retrieved using the untruncated-moment method. Further analysis of raindrop spectra revealed that the correlation between μ and Λ is also reduced due to incomplete sampling of DSD as a result of the finite sampling volume of the video disdrometer within a 1-min sample time. To minimize the error due to sampling effects, data were filtered by allowing only those with rain rate >5 mm h^{-1} and the number of raindrops $N_T > 1000$ m^{-3}. The revised plot with the above-mentioned threshold is shown in Figs. 5c and 5d. The figures contain only 248 data points but captured 75% of the rainfall amount in Figs. 5a and 5b. The scatterplots shown in Figs. 5c and 5d show less scatter, and the correlation between μ and Λ is higher. A relation between Λ and μ is estimated using a polynomial least squares fit, and it is given as

$$\Lambda = 0.037\mu^2 + 0.691\mu + 1.926 \text{ mm}^{-1}, \tag{9}$$

when untruncated moments are used. In the case of the truncated-moment method, the corresponding equation is

$$\Lambda = 0.0365\mu^2 + 0.735\mu + 1.935 \text{ mm}^{-1}. \tag{10}$$

It is interesting to note that the μ and Λ relations do not change much while the mean values of μ and Λ change from 4.09 and 5.58 in Fig. 5c to 3.25 and 4.92 in Fig. 5d for the truncated-moment method.

To include more DSD samples with valid fitted DSD parameters, we increased the sampling time for each DSD from 1 to 3 min and found a very similar μ–Λ relation to (10) as long as the threshold of $R > 1$ mm h^{-1} and $N_T > 1000$ m^{-3} is imposed. In this case, 91% of rain accumulation and 44% of DSD samples are included. The rest of the measured DSD correspond to either very light rain that has little contribution to total rain accumulation or a small number of drop counts that could lead to large errors in estimated DSD parameters.

A fixed-power law equation, such as $Z = AR^b$, rep-

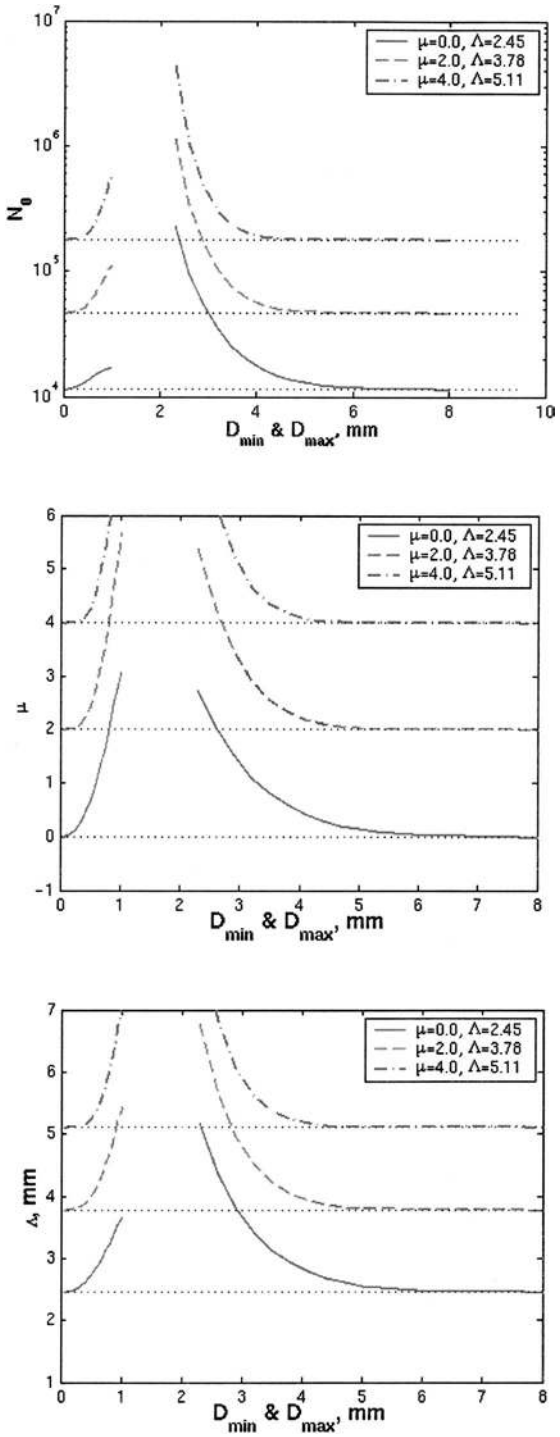

FIG. 2. Effect of truncated moments in estimating the gamma DSD parameters. The retrieved DSD parameters shown as a function of the lower limit D_{min} and upper limit D_{max} of the spectrum. All three DSD parameters (top) N_0, (middle) μ, and (bottom) Λ increase as the spectrum is truncated (increase in D_{min} or decrease in D_{max}), that is, as the spectrum becomes narrower. Thus, usage of truncated moments instead of untruncated moments in Eqs. (3), (4), and (5) introduces significant error in the estimated DSD parameters.

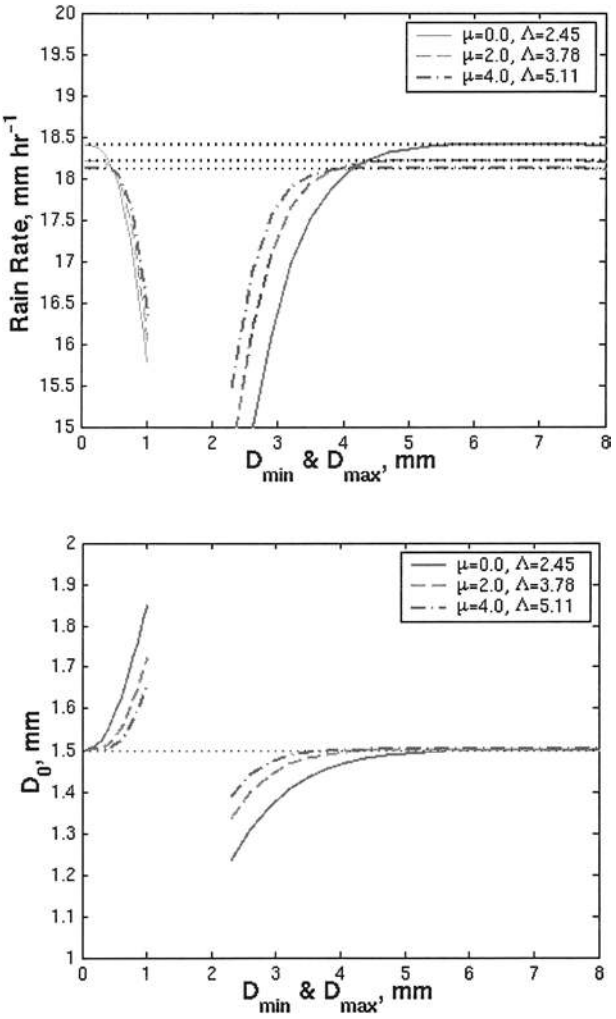

FIG. 3. Same as Fig. 2, except truncation effects on (top) rain rate and (bottom) median volume diameter calculated from fitted gamma DSD parameters are shown.

resents very limited variability in DSD. For a gamma DSD, the parameters N_0, μ, and D_0 can be derived using A and b power-law coefficients as (Rosenfeld and Ulbrich 2003)

$$N_0 = \left\{ \frac{A\left[33.31\Gamma\left(\frac{2.33}{b-1}\right)\right]^b}{10^6\Gamma\left(\frac{2.33b}{b-1}\right)} \right\}^{1/(1-b)}, \quad (11a)$$

$$\mu = \frac{7 - 4.67b}{b-1}, \quad \text{and} \quad (11b)$$

$$D_0 = \frac{3.67 + \mu}{[33.31N_0\Gamma(4.67+\mu)]^{1/(4.67+\mu)}} R^{1/(4.67+\mu)} \text{ mm}. \quad (11c)$$

The above relations show that for a specified power-law equation, N_0 and μ are fixed, and that the range of D_0

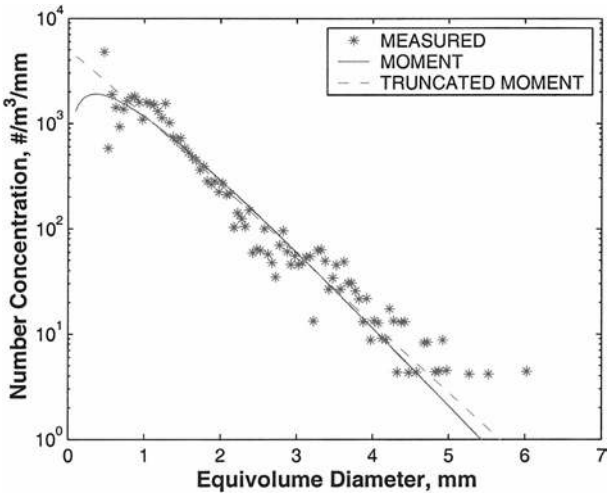

FIG. 4. An example of measured rain DSD and its fitted gamma distribution using the moment and the truncated-moment method. The gamma DSD parameters are different for untruncated and truncated methods, and corresponding values of N_0, μ, and Λ are (7332, 0.67, 1.85) and (5441, 0.031, 1.53), respectively. Even though truncated- and untruncated-moment methods produce similar rain rate and D_0, the corresponding DSD parameters are different.

is also limited. Assuming each *Z–R* power-law equation represents average DSD parameters of a particular rain event, it might be interesting to compare the inferred DSD parameters with a μ–Λ relation. Twenty-three different *Z–R* power-law relations listed in Table 5 of Rosenfeld and Ulbrich (2003) represent a wide range of precipitation events: continental, tropical continental, tropical maritime, hurricane, and orographic. Using the above equations and the $\Lambda = (3.67 + \mu)/D_0$ relation, where D_0 was obtained as a function of rain rate, Λ and μ were calculated for each *Z–R* power law. Figure 6 shows a scatterplot of μ and Λ for 23 *Z–R* relations, and they are scattered along the μ–Λ line. Given the likely differences in 23 field experiments, the general agreement of the scatterplot with the μ–Λ relation is gratifying. This result shows that each *Z–R* power relation can only represent a subset of rain DSDs with a very limited coverage of rain process. The result suggests that independent of rain type, a large mean drop size corresponds to broad DSD, except that the μ and Λ points, corresponding to an orographic *Z–R* rain event, exhibit maximum deviation from the mean μ–Λ line, suggesting that the rain DSD is dominated by a condensation process that is different from all other types of rain. The μ–Λ relation of an orographic precipitation event may be much different from the one discussed in this paper.

It is also important to discuss whether the μ–Λ relation arises from errors in an estimated DSD moment or from natural rain processes. This situation is discussed in a detailed error analysis in a recent paper (Zhang et al. 2003). The research shows that the statistical errors do induce correlations in estimated DSD parameters and cause a linear relation between μ and Λ estimates. However, the slope and intercept of the error-induced relation depend on the expected values of μ and Λ of individual DSDs, and as a result no relation between μ and Λ is inferred for a random set of DSDs. It was shown that the moment-fitting procedure does not cause a bias in the DSD parameters and does not amplify the errors in rain physical parameters (R and D_0). It may be argued that the μ–Λ relation is due to the fact that μ and Λ are related by $\Lambda D_0 = \mu + 3.67$, while D_0 is usually within a small range (1–2.5 mm). The finite range of D_0 can cause a correlation between μ and Λ but does not necessarily lead to the μ–Λ relation, as shown in Fig. 6b of Zhang et al. (2003). A physical explanation is that the width of a raindrop spectrum and the characteristic drop size, such as D_0, are correlated. It can be shown that the width and D_0 of a gamma DSD are nonlinearly related for natural rain DSDs and are equivalent to the nonlinear μ–Λ relation described in Eq. (10). However, in the case of a gamma DSD with fixed μ, the width and D_0 are linearly related. The constrained gamma distribution with the μ–Λ relation is more flexible in representing a wide range of instantaneous DSD shapes. Analysis of equilibrium and/or steady-state DSDs reported in a number of earlier studies are in agreement with the μ–Λ relation (Zhang et al. 2001). Therefore, this information is useful in rain DSD retrieval from limited remote measurements. The μ–Λ relation reduces a gamma DSD to only two parameters and simplifies DSD retrieval using Z and Z_{DR}. The polarization radar–based estimators, using constrained gamma DSD for retrieving rain rate, median drop size, specific propagation phase, attenuation, and differential attenuation, are discussed in the following two sections.

4. Constrained gamma DSD

a. Shape of constrained gamma DSD

It is interesting to compare a DSD and mass spectrum for fixed liquid water content (LWC) of 1 g m^{-3} for μ of 0, 2, 4, and 8. Using the μ–Λ relation in Eq. (10), the corresponding D_0 are 1.90, 1.73, 1.60, and 1.15 mm, respectively. The results are plotted and shown in Fig. 7. Figure 7a is the distribution of DSDs and Fig. 7b is that of the mass spectrum. The rain DSD with large (small) μ corresponds to small (large) D_0 and a narrow (broad) mass distribution. Parameter μ (or Λ) determines both the shape and the slope, while parameter Λ in an exponential distribution only adjusts the slope.

b. Raindrop size

The characteristic size of the DSD is an important parameter and can be defined in various ways. In general, any pair of moments can be used to define the characteristic size for a specific rain DSD as

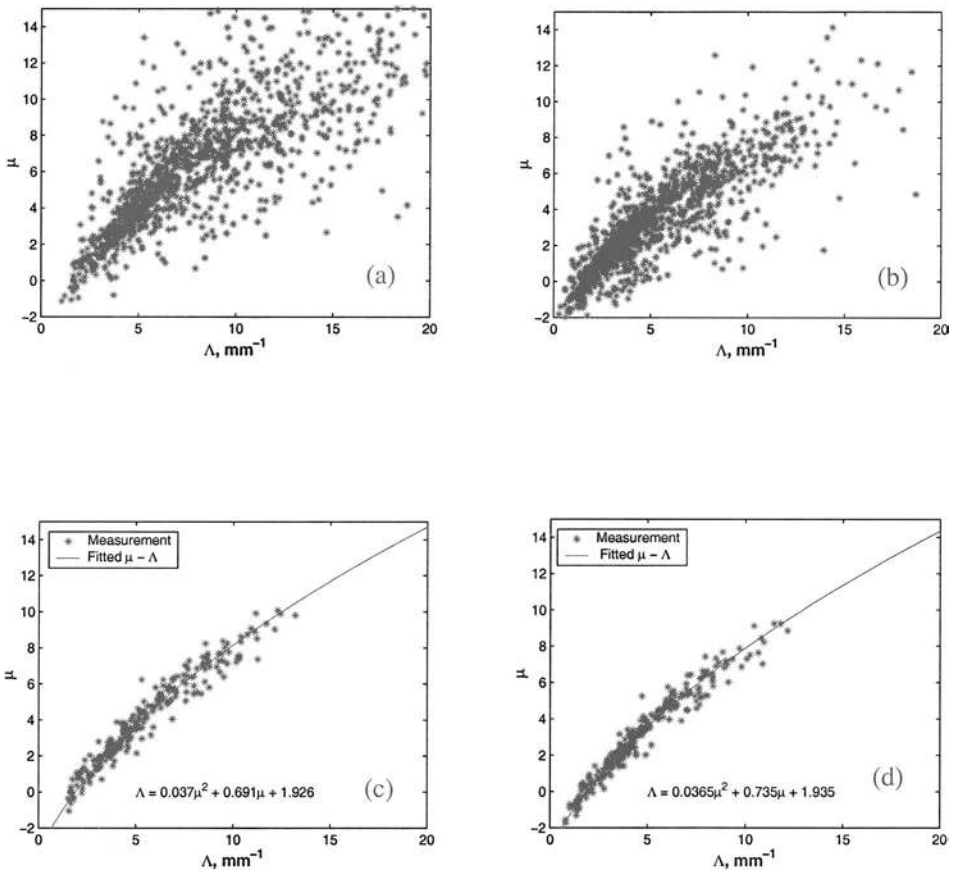

FIG. 5. Scatterplots of μ–Λ values obtained from video-disdrometer observations using the moment method and the truncated-moment method. (a) Untruncated-moment method Eqs. (3)–(5); (b) truncated-moment method Eqs. (7)–(8); (c) same as (a), except including measured DSDs only for $R > 5$ mm h^{-1} and total raindrop counts>1000; and (d) same as (c), except including measured DSDs only for $R > 5$ mm h^{-1} and total raindrop counts >1000.

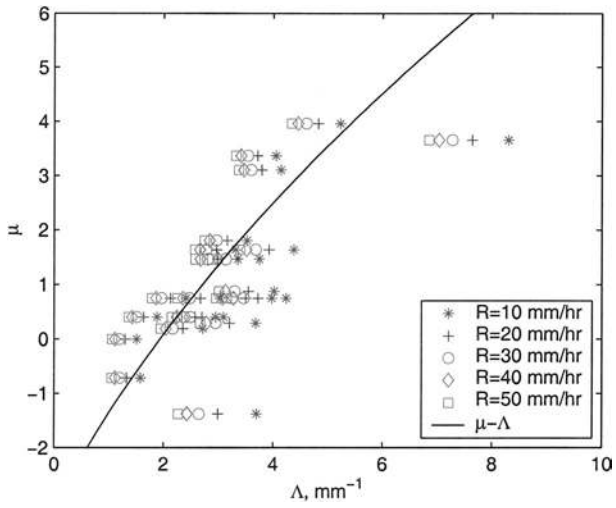

FIG. 6. Scatterplot of μ–Λ values corresponding to 23 different Z–R relations described in Rosenfeld and Ulbrich (2003). The Z–R relations represent a wide range of precipitation events: continental, tropical continental, tropical maritime, hurricane, and orographic. The solid line is the μ–Λ relation.

$$D_g = \left(\frac{\langle D^{n+m}\rangle}{\langle D^n\rangle}\right)^{1/m}. \quad (12a)$$

In the case of constrained gamma DSD, it is written as

$$D_g = [\Lambda(\mu)]^{-1}\left[\frac{\Gamma(\mu + n + m + 1)}{\Gamma(\mu + n + 1)}\right]^{1/m}, \quad (12b)$$

which depends only on the shape parameter μ of the DSD.

In practice, however, only those characteristic sizes that are physically meaningful and particularly estimated using remote measurements should receive the most attention and be studied thoroughly. Median volume diameter (D_0) is commonly used to characterize raindrop size because the total mass of raindrop sizes smaller than D_0 and greater than D_0 are equal. Mean mass diameter D_m is also used because it is mass weighted and can be easily calculated from the third and fourth moments. Mass mode diameter D_c indicates the location of the peak of the mass distribution of DSD. Recently, radar-estimated size (RES) for a dual-wavelength radar

technique and a size parameter for polarimetric radar technique were proposed (Vivekanandan et al. 2001; Zhang et al. 2001). RES is defined as the ratio of the 7.2th and sixth moments. Because the 7.2th moment is proportional to the linear reflectivity difference Z_{DP}, while the sixth moment is the reflectivity factor, RES can be directly determined from polarimetric radar measurements. Thus, in the case of a constrained gamma DSD, various characteristic sizes can be expressed as follows:

$$\mathrm{RES} = \left(\frac{\langle D^{7.2}\rangle}{\langle D^{6}\rangle}\right)^{1/1.2} = \frac{1}{\Lambda(\mu)}\left[\frac{\Gamma(\mu + 8.2)}{\Gamma(\mu + 7)}\right]^{1/1.2}, \quad (13)$$

$$D_m = \frac{\langle D^4\rangle}{\langle D^3\rangle} = \frac{\Gamma(\mu + 4)}{\Lambda(\mu)\Gamma(\mu + 3)}, \quad (14)$$

$$D_0 = \frac{\mu + 3.67}{\Lambda(\mu)}, \quad \text{and} \quad (15)$$

$$D_c = D|_{[dm(D)]/dD=0} = \frac{\mu + 3}{\Lambda(\mu)}. \quad (16)$$

The width of the DSD is also important in characterizing the shape of the spectrum. As shown in Ulbrich (1983), the variance of the mass distribution with respect to D_m is given as

$$\sigma_D^2 = \frac{\int (D - D_m)^2 D^3 N(D)\, dD}{\int D^3 N(D)\, dD} = \frac{\mu + 4}{[\Lambda(\mu)]^2}. \quad (17)$$

Figure 8 shows the dependence of characteristic size and variance on the shape parameter μ. Radar-estimated size RES, mean mass diameter D_m, median volume diameter D_0, and mass mode diameter D_c are shown, as well as the variances. They all decrease as μ increases. These results are consistent with the radar and disdrometer observation that generally large Z_{DR} corresponds to large drop size and broad distribution (small μ) in actual radar measurement. The limited video-disdrometer observations show that Z_{DR} varies between 0 and 2.5 dB for rain rates between 5 and 80 mm h^{-1} (Brandes et al. 2002; Zhang et al. 2001). Video-disdrometer measurements show that broad DSD spectrum tends to have large D_0 (Zhang et al. 2001). However, in the leading edge of a convective storm Z_{DR} can be much larger than 2.5 dB (i.e., 3–4 dB) and they are associated with a low concentration of very large drops (Illingworth et al. 1987). A constrained gamma DSD model may not be appropriate to characterize DSDs corresponding to 3–4 dB Z_{DR} at the leading edge of convective storms.

5. Polarimetric radar–based estimators

As discussed in the previous section, three parameters of gamma DSD are difficult to retrieve from a set of limited radar measurements. The relation $\Lambda(\mu)$ or $\mu(\Lambda)$ derived in the previous section constitutes a constrained condition for gamma distribution. The μ–Λ relation applied to gamma DSD [Eq. (1)] reduces to a two-parameter DSD and is dubbed as a constrained gamma DSD.

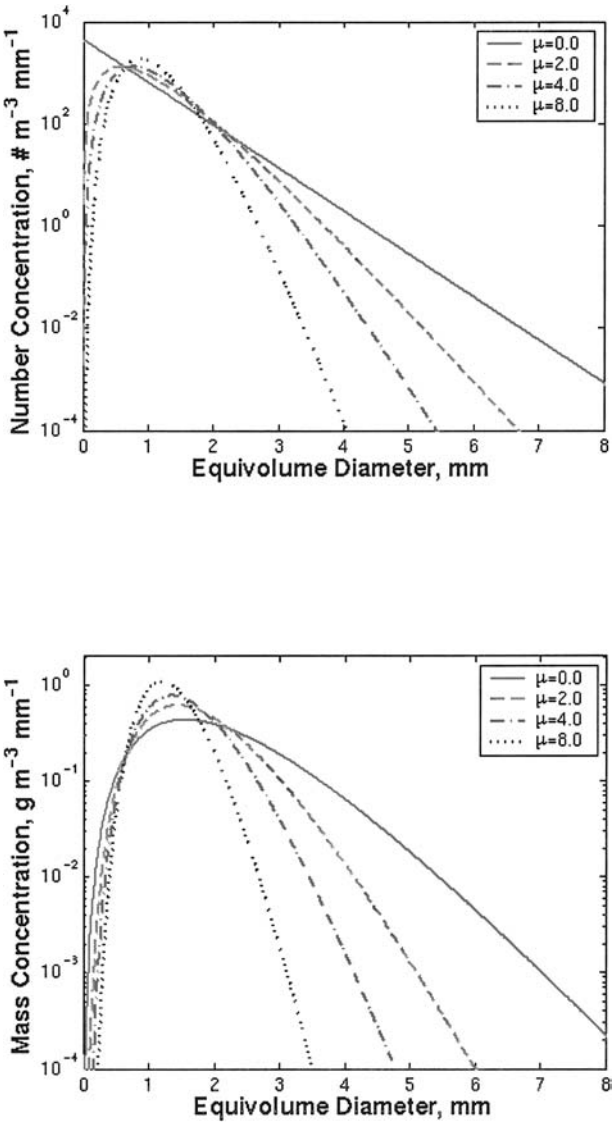

FIG. 7. Constrained gamma raindrop size distribution for a fixed mass content of 1 g m^{-3}: (top) number concentration and (bottom) mass concentration. Large μ (and Λ) produce large curvature in both DSDs and mass spectra with narrow distribution. Parameter μ (or Λ) determines both the shape and the slope, while parameter Λ in an exponential distribution only adjusts the slope. The constrained gamma DSD might be flexible enough to characterize rain DSD.

a. Raindrop shape

Even though the μ–Λ relation simplifies the DSD retrieval, any difference between assumed and actual microphysical parameters such as shape and canting angle might introduce uncertainties in a polarization radar-

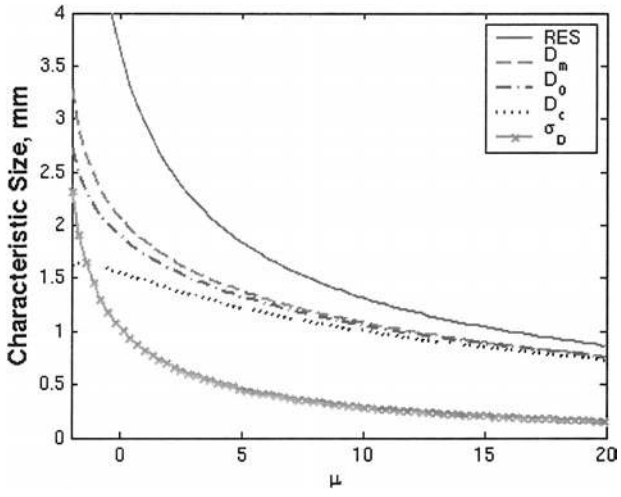

FIG. 8. Dependence of characteristic size and variance on the shape parameter μ. Radar-estimated size RES, mean mass diameter D_m, median volume diameter D_0, and mass mode diameter D_c are shown, as well as the standard deviation of DSD. They all decrease as μ increases. This is consistent with the radar and disdrometer observations: large Z_{DR} corresponds to large drop size and broad distribution (small μ) in actual radar measurements. The phrase "large Z_{DR}" in this paper refers to relatively high Z_{DR} values between 0.0 and 2.5 dB.

based retrieval. An equilibrium shape of raindrops is assumed in some earlier studies, while the latest observations suggest that a more spherical shape should be adapted. There has been considerable discussion about the deviation of the drop axis ratio from its equilibrium value (Chandrasekar et al. 1988; Beard and Kubesh 1991; Bringi et al. 1998; Beard and Chuang 1987; Andsager et al. 1999; Keenan et al. 2001). We used a smooth curve that optimally describes the results in Pruppucher and Pitter (1971), Chandrasekar et al. (1988), Beard and Kubesh (1991), and Andsager et al. (1999). We extended the results to smaller diameters with a smooth polynomial. The polynomial fit is made by assuming that the drop axis ratio merges smoothly with the equilibrium axis ratio in the larger diameter regime. The proposed polynomial fit can be represented (Brandes et al. 2002) as

$$r = 0.9951 + 0.025\,10D - 0.036\,44D^2 + 0.005\,030D^3 - 0.000\,249\,2D^4, \quad (18)$$

where r is the drop axis ratio and D is the equivolume drop diameter (mm).

b. Relations among statistical moments

Statistical moments are integral parameters of a DSD. They are directly related to polarization radar measurements and rainfall rate. When radar wavelength is large compared to raindrop size, as in the case of S-band radar measurements of rain, the reflectivity factor is the sixth moment ($Z = \langle D^6 \rangle$). Rain rate is related to the 3.67th moment ($R \sim \langle D^{3.67} \rangle$). It is important to know the relation among the moments that can be used to relate radar measurements and various rain parameters. Instead of eliminating the median volume diameter, as in Ulbrich (1983) and Testud et al. (2001), the relation between two moments can be obtained by eliminating N_0. Therefore, a relation between the kth and lth moments of a constrained gamma DSD can be found by taking a ratio as

$$\frac{\langle D^k \rangle}{\langle D^l \rangle} = \Lambda(\mu)^{-(k-l)} \frac{\Gamma(\mu + k + 1)}{\Gamma(\mu + l + 1)}, \quad (19)$$

that is,

$$\langle D^k \rangle = \Lambda(\mu)^{-(k-l)} \frac{\Gamma(\mu + k + 1)}{\Gamma(\mu + l + 1)} \langle D^l \rangle. \quad (20)$$

It should be pointed out that Eq. (20) does not specify a linear relation between the moments. Actually it does not even guarantee a functional relation because all of the moments depend on μ, which is a variable. A linear relation exists only when the shape of DSD is fixed, such as the equilibrium shape of DSD (List 1988) or constrained gamma DSD with a constant μ in Eq. (20). The shape of DSD (or μ), however, usually depends on characteristic size and should not be treated as a constant.

Generally, rain rate R (mm h^{-1}) is proportional to the 3.67th moment as

$$R = 7.125 \times 10^{-3} \langle D^{3.67} \rangle. \quad (21)$$

Letting $k = 3.67$ and $l = 6$ in Eq. (20) and substituting into (21),

$$R = 7.125 \times 10^{-3} F(\mu) Z \text{ mm h}^{-1}, \quad (22)$$

where

$$F(\mu) = [\Lambda(\mu)]^{2.33} \frac{\Gamma(\mu + 4.67)}{\Gamma(\mu + 7)}. \quad (23)$$

This shows that the Z–R relation is governed by the shape parameter μ. For a constrained gamma DSD, μ uniquely determines Z_{DR} (Zhang et al. 2001) for the assumed axis ratio and mean canting angle of raindrops. Considering that Z may not be exactly the 6th moment of DSD, even when particle size is small in comparison with wavelength, the rain estimator is derived as follows: rain DSDs are constructed with a fixed N_0 and varying Λ from 1.5 to 9.5 mm^{-1}, and the corresponding μ is calculated from Eq. (10). Then, the rain parameters (R and D_0) are calculated from the rain DSDs and polarimetric radar measureables Z, Z_{DR}, K_{DP}, attenuation A, and differential attenuation ΔA are obtained using a rigorous T-matrix-based scattering calculation.

For rain-rate estimation, a least squares fit is obtained between the logarithm of the ratio R/Z and the logarithm of Z_{DR}, where Z_{DR} is in linear units. The first-order linear relation between logarithm quantities is rewritten as

$$R = 4.75 \times 10^{-3} Z Z_{DR}^{-b_R} \text{ mm h}^{-1}, \quad (24)$$

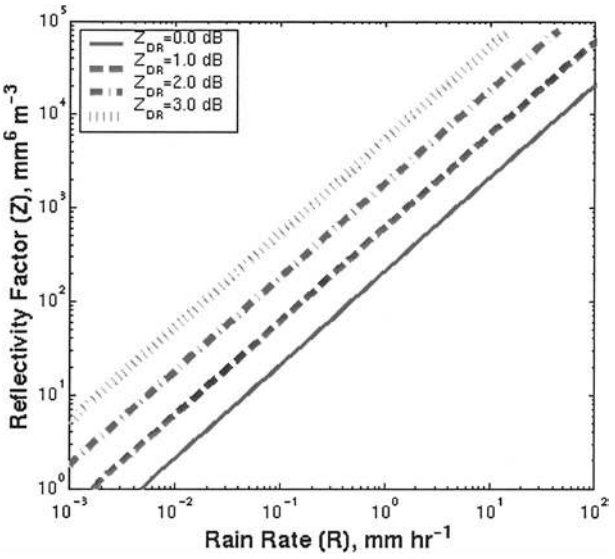

FIG. 9. Relation between reflectivity and rain rate for various differential reflectivity factors. Larger Z_{DR} corresponds to small μ. Specification of Z_{DR} confines the $Z(R)$ relation to smaller ranges of rain rate than a typical larger scatter in $Z(R)$ relations. The thickness of each line represents the margin due to the effective canting angle of raindrops.

where the exponent b_R depends on the effective canting angle of raindrops. In the case of a Gaussian canting angle distribution, assuming the mean canting angle is zero, the coefficient b_R is expressed as a function of the standard derivation of an effective canting angle (σ_ϕ) as

$$b_R = 4.685 - 0.602\sigma_\phi + 12.032\sigma_\phi^2, \qquad (25)$$

where σ_ϕ is in radians, which can be estimated from cross-polarization radar measurements (Ryzhkov et al. 1999). However, it should be noted that the technique for estimating the standard deviation of the effective canting angle from polarimetric radar measurements is exploratory and has not been sufficiently demonstrated for general applicability throughout a convective echo. As compared with the widely used relation $R = 6.86 \times 10^{-3} Z Z_{DR}^{4.86}$ (Sachidananda and Zrnić 1987), Eq. (24) has a smaller coefficient and higher value of exponent for Z_{DR}. The use of a less oblate raindrop shape in the radar-scattering calculation is a primary factor that made significant improvement to the Z_{DR}-based rain estimator. However, both the less oblate shape and the μ–Λ relation (instead of fixed μ) contribute to the improvement of rain estimation. For example, even in the case of less oblate shapes, the ratio between gauge- and radar-based rain estimates changes from 0.83 to 1.03 as μ changes from 0 to 4 (Brandes et al. 2003). Figure 9 shows the relation between Z and R for various Z_{DR}. For a specified Z, Eq. (24) gives a higher rain rate for a smaller Z_{DR} than with a larger Z_{DR}, because small Z_{DR} is related to a larger amount of smaller raindrops. Specification of Z_{DR} confines the Z–R relation constrained to smaller ranges of rain rate than a typical larger scatter in Z–R relations (Doviak and Zrnic 1993; Ulbrich and Atlas 1998).

Even though no detailed comparison between radar R and gauge G estimates was discussed in this paper, we evaluated the performance of Eq. (24) when varying the standard deviation of canting angle between 0° and 15°. The rain-rate estimators in Brandes et al. (2002, 2003) assumed $\sigma_\phi = 0°$, and the corresponding G/R values are 0.97 and 0.93, respectively. The G/R for the same set of observations increases from 0.87 to 1.02 as σ_ϕ is increased from 0° to 15° when Eq. (24) is used. Realizing the difficulty in separating the effect of drop shape from canting angle using liner polarization radar measurements, σ_ϕ can be considered as a tuning parameter.

For rain estimation from a specific propagation phase, the relation of $R = 40.56 K_{DP}^{0.866}$ (Sachidananda and Zrnić 1987) tends to underestimate rain, especially for low rainfall (Brandes et al. 2001, 2003). Recently, Z_{DR} was combined with K_{DP} to reduce the effects due to an apparent change in drop shape as a result of canting and oscillation (Ryzhkov and Zrnić 1995). Similar to the procedure for deriving the $R(Z, Z_{DR})$ relation, a physically based $R(K_{DP}, Z_{DR})$ relation can be obtained by fitting the ratio R/K_{DP} as a function Z_{DR} as

$$R = \frac{143.18}{(1 - 2\sigma_\phi^2)} K_{DP} Z_{DR}^{-(2.629 - 0.361\sigma_\phi + 7.435\sigma_\phi^2)} \text{ mm h}^{-1}. \qquad (26)$$

For a comparable K_{DP} and Z_{DR}, rain-rate estimation using the above equation is 10%–15% higher than the earlier rain-rate estimator reported in Gorgucci and Scarchilli (1997).

Again, we evaluated the performance of Eq. (26), varying the standard deviation between 0° and 15°. The G/R, that is, the mean bias factor, is 0.82, when $\sigma_\phi = 0°$ and it gradually decreases to 0.79 when $\sigma_\phi = 15°$. Thus, the effect of σ_ϕ on $R(K_{DP}, Z_{DR})$ is minimal. Brandes et al. (2002) assumed $\sigma_\phi = 0°$ with a corresponding G/R of 0.92; the G/R for Eq. (26) is 0.82. This difference is mainly due to the DSD because the same mean raindrop shape is assumed in all of the calculations. The Brandes et al. (2002) $R(K_{DP}, Z_{DR})$ relation is based on the in situ video-disdrometer DSD collected during the PRECIP98 field program. However, the $R(K_{DP}, Z_{DR})$ relation presented in this paper is based on a constrained gamma DSD, and no in situ DSDs are included explicitly. Thus, the $R(K_{DP}, Z_{DR})$ presented in this paper might be more appropriate when no information regarding DSD is available to fine-tune the $R(K_{DP}, Z_{DR})$ estimator.

Similarly, closed-form analytical relations for a median volume diameter, specific propagation phase, specific attenuation A_H, and a differential attenuation ΔA are derived as follows:

$$D_0 = 1.017 + (0.448 - 0.064\sigma_\phi + 1.278\sigma_\phi^2) \times Z_{DR}(\text{dB}) \text{ mm} \quad \text{for } Z_{DR} \geq 0.2 \text{ dB}, \qquad (27)$$

$$K_{DP} = 3.32 \times 10^{-5}(1 - 2\sigma_\phi^2) \times Z Z_{DR}^{-(2.053 - 0.107\sigma_\phi + 4.135\sigma_\phi^2)} \ ^\circ \text{ km}^{-1}, \quad (28)$$

$$A_H = \frac{5.29 \times 10^{-2}}{(1 - 2\sigma_\phi^2)} \times K_{DP} Z_{DR}^{-(2.483 - 0.384\sigma_\phi + 7.663\sigma_\phi^2)} \text{ dB km}^{-1}, \quad \text{and} \quad (29)$$

$$\Delta A = 2.22 \times 10^{-3} K_{DP} Z^{1.033 - 0.144\sigma_\phi + 2.937\sigma_\phi^2} \text{ dB km}^{-1}, \quad (30)$$

where K_{DP} is in degrees per kilometer and Z_{DR} is in linear units unless specified in decibels. Note that Eq. (27) for estimating D_0 is valid only when Z_{DR} is greater than or equal to 0.2 dB. Specific differential phase K_{DP} is an important parameter, which can be used for checking self-consistency among Z, Z_{DR}, and K_{DP}. Equations (29) and (30) can be used to compensate any bias in reflectivity and Z_{DR} due to rain attenuation. In the following section, the above-derived expressions are used for estimating rain DSDs and also for verifying consistency in polarization radar measurements when the Λ–μ relation is used.

6. Rain DSD retrievals and consistency of the Λ–μ relation

During PRECIP98, NCAR's S-Pol radar was deployed to evaluate the potential of a polarimetric radar for estimating rain in a tropical environment. Rain gauge measurements were also collected during the project. A detailed description of the project and instrument deployment is reported in Brandes et al. (2002). A preliminary analysis of data collected during this experiment is presented in the following sections to show the utility of constrained gamma DSD–based estimators and indirect verification of radar-based estimators presented in this paper. A constrained gamma DSD is completely specified by Z and Z_{DR}, and it also facilitates formulation of polarimetric-radar estimators for retrieving DSD parameters, rain rate, attenuation, and specific propagation phase.

a. Spatial description of DSD

Figure 10 shows a vertical cross section collected at 1901 UTC on 17 September, 1998. Figures 10a and 10b are radar reflectivity and Z_{DR}, respectively. There are two well-developed storms centered at 26 and 45 km, respectively, as shown in the Z and Z_{DR} images. Positive Z_{DR} suggests that most of the precipitation between the ground and 5 km AGL is rain. Using the relations shown in an earlier section, parameters of DSD were calculated. For a specified Z_{DR}, the median diameter is obtained from Eq. (27) and then μ and Λ can be obtained from Fig. 8 and Eq. (10). The parameter N_0 is retrieved from Z, Λ, and μ, using the relation $N_0 = Z\,\Lambda^{\mu+7}/\Gamma(\mu + 7)$ and then N_T is equal to $N_0\,\Lambda^{-(\mu+1)}\Gamma(\mu + 1)$. Rain rate is calculated from Eq. (24). Figures 10c and 10d are retrieved rain DSD parameters, namely, the total number concentration N_T and shape parameter μ. Maximum raindrop concentration exceeds 1000 m^{-3} and μ values are less than 2 in the regions that have large drop concentrations. Rain cell boundaries are characterized by large μ, that is, a narrow DSD with smaller concentrations of raindrops. Thus, high-reflectivity regions correspond to large number concentrations and a broad raindrop spectrum. Figures 10e and 10f are calculated rain characteristics, that is, rain rate R and median volume diameter. The rain rate is derived from the estimated DSD parameters instead of a fixed power-law-type equation, and the peak rain rates are around 100 mm h^{-1}. Median volume diameter values are larger in regions of heavier precipitation and they are smaller than 1.5 mm near the cell boundaries.

b. Self-consistency in polarization radar measurements when using constrained gamma DSD

To verify the validity of constrained gamma–based polarization radar estimators, self-consistency in polarization observation is used. We compare the estimated differential phase and specific differential phase with those measured (Vivekanandan et al. 2003). The estimated specific propagation phase (K_{DP}^e) is obtained from power measurements; that is, Z and Z_{DR}, using Eq. (28) with a specified $\sigma_\phi = 0^\circ$ (Ryzhkov et al. 1999), and the estimated propagation phase (ϕ_{DP}^e) is calculated as $\phi_{DP}^e = 2 \int K_{DP}^e(l)\, dl$, where l is the distance along the radial for one of the radar rays. Figure 11 shows comparisons of a differential propagation phase between measurements and estimations. Figure 11a is an example of differential phase plotted as a function of range. As expected, estimated ϕ_{DP} monotonically increases with range and agrees well with the mean of the measurement. The statistical comparison is shown in the scatterplot in Fig. 11b. There are 60 rays and 6104 data points. The mean of the measured ϕ_{DP} is 11.73° and the mean of the estimated value is 11.45°. Good agreement between measured and estimated ϕ_{DP} indirectly verifies the constrained gamma DSD–based polarimetric radar estimators.

7. Summary and discussion

The constrained condition (μ–Λ relation) was derived from video-disdrometer measurements. Effects of truncated moments on estimating DSD parameters from video-disdrometer measurements are discussed. It is shown that as long as $D_{min} < 0.5\ D_0$ and $D_{max} > 4\ D_0$ are satisfied, the effect of truncation on retrieved parameters is less than 5%. When truncated moments are used, an iterative approach is required in estimating the DSD parameters. Retrieved μ and Λ DSD parameters from a video-disdrometer observation using truncated moments show a strong correlation between μ and Λ. The two-parameter DSD allows the retrieval of DSD param-

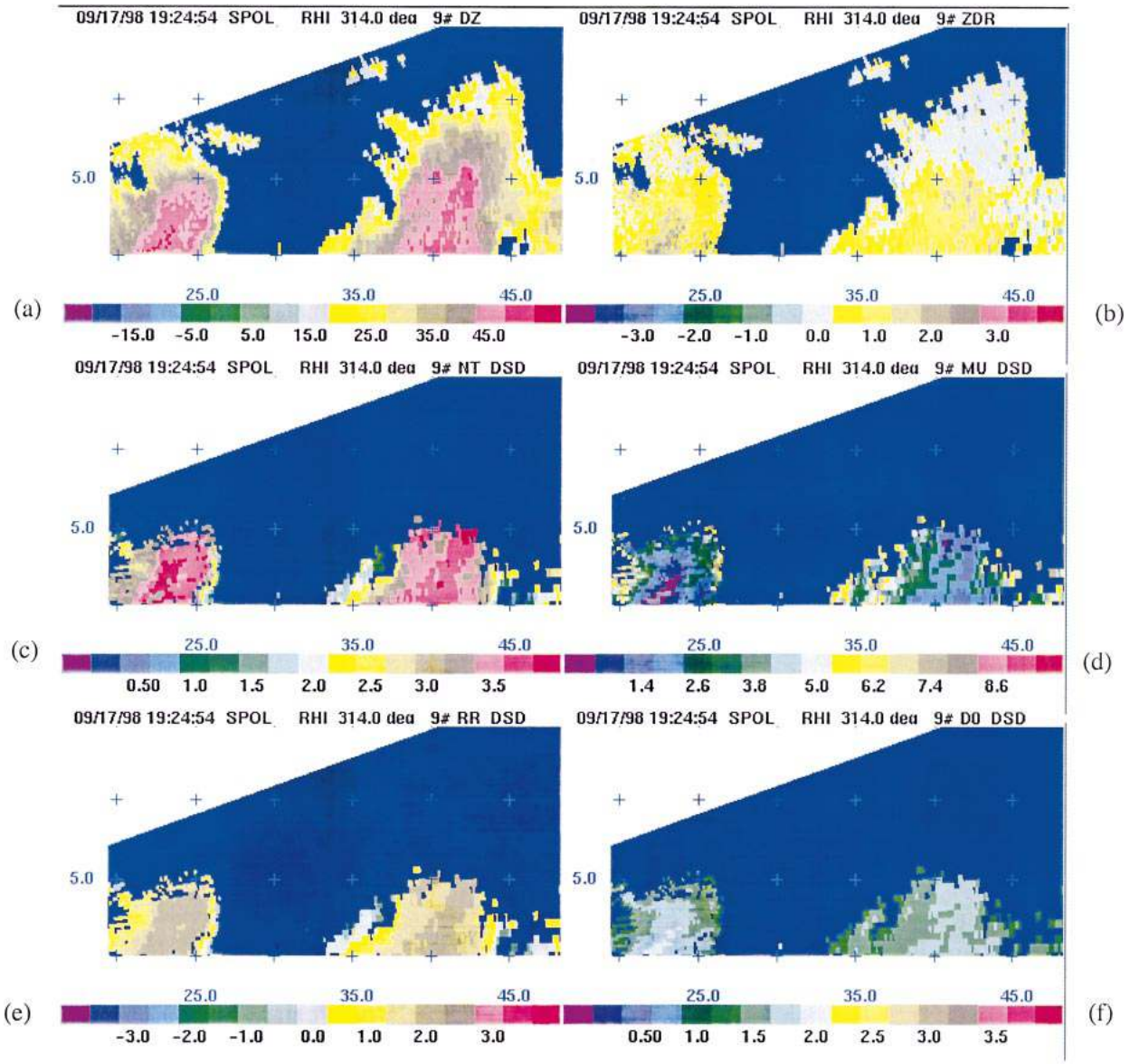

FIG. 10. Spatial distribution of polarization radar measurements, retrieved DSD parameters, and rain rate: (a) reflectivity, (b) differential reflectivity, (c) number concentration (m^{-3}), (d) μ, (e) DSD-based $\log_{10}$ of rain rate (mm h^{-1}), and (f) median volume diameter (mm). Note $\log_{10}$ of number concentration and rain rate are shown. Standard deviation of canting angle σ_ϕ is assumed to be 10°.

eters from polarization radar measurements: reflectivity and differential reflectivity.

In the case of constrained gamma DSD, characteristic size and variance of size depend only on the shape parameter μ. Radar-estimated size RES, mean mass diameter D_m, median volume diameter D_0, mass mode diameter D_c, and standard deviation of the DSD σ_D are derived as a function of μ. All characteristic sizes decrease as μ increases. This result is consistent with the radar and disdrometer observations: large Z_{DR} correspond to large drop size and broad distribution (small μ) in actual radar measurement. It is shown that a μ–Λ relation is consistent with rain physics by representing large drops with broad distribution.

Polarimetric radar estimators for rain rate, median volume diameter, specific propagation phase, specific attenuation, and differential attenuation are derived for S-band radar observations. The equations assume zero mean and variable standard deviation of canting angle. These expressions will be useful in analyzing radar data and also calibrating radar reflectivity. A preliminary analysis of range–height indicator radar measurement is presented and spatial variation of DSD parameters is discussed. Excellent agreement between a measured

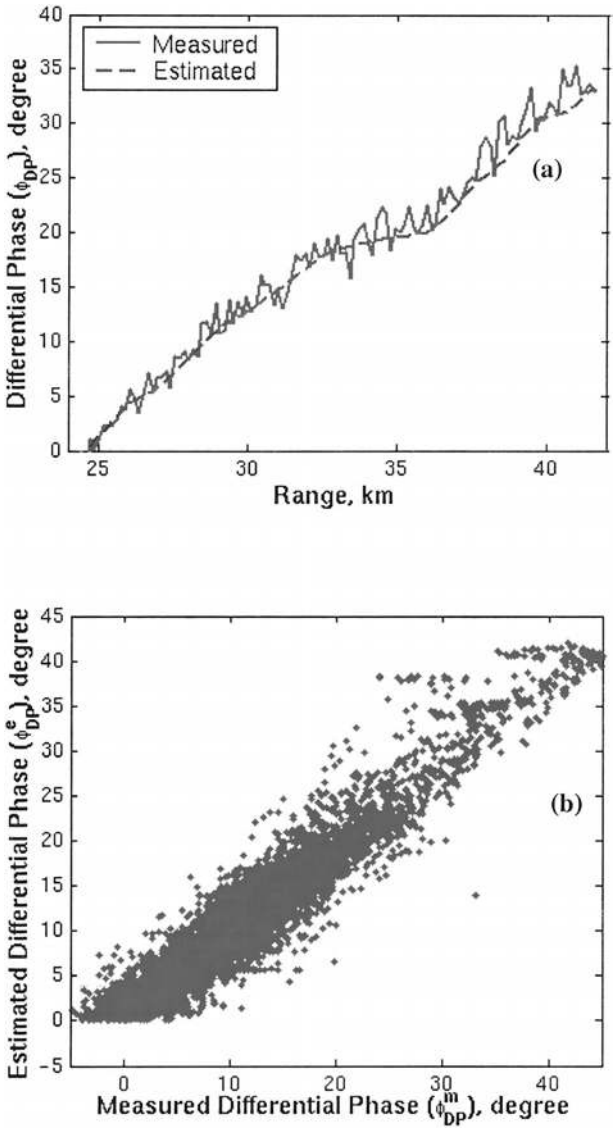

FIG. 11. Indirect verification of μ–Λ relation and self-consistency among polarization radar observations. (a) An example of measured and estimated ϕ_{DP} along a radar beam, and (b) scatterplot of measured and estimated ϕ_{DP} for a number of radar beam segments.

propagation phase and that derived based on constrained DSD, indirectly verifies the polarimetric radar estimators presented in this study.

Polarimetric measurements are sensitive to DSD, shape, and canting angle. Even though the μ–Λ relation simplifies DSD retrieval, any difference between assumed and actual microphysical parameters, such as shape and canting angle, might introduce uncertainties in the polarization radar–based retrieval. As compared with a three-parameter gamma distribution with a fixed μ, the constrained gamma distribution with the μ–Λ relation is more flexible in representing a wide range of instantaneous DSD shapes. The μ–Λ relation reduces a gamma DSD to a two-parameter function and simplifies DSD retrieval using Z and Z_{DR}. Even though all types of rain DSD may exhibit correlation between μ and Λ, it is important to analyze DSDs collected at various geographical locations and in various seasons to understand the variability in the μ–Λ relation.

Acknowledgments. The authors thank Witold F. Krajewski and Anton Kruger of The University of Iowa for making the video-disdrometer data available. The authors also thank J. Lutz and M. Randall of NCAR/ATD for smooth operation of the S-Pol radar. Carol Park, of the National Center for Atmospheric Research, formatted the manuscript and provided general editorial assistance. The study was partly supported by funds from the National Science Foundation, designated for the U.S. Weather Research Program at National Center for Atmospheric Research (NCAR).

REFERENCES

Andsager, K., K. V. Beard, and N. F. Laird, 1999: Laboratory measurements of axis ratios for large drops. *J. Atmos. Sci.,* **56,** 2673–2683.

Beard, K. V., and C. Chuang, 1987: A new model for the equilibrium shape of raindrops. *J. Atmos. Sci.,* **44,** 1509–1524.

——, and R. J. Kubesh, 1991: Laboratory measurements of small raindrop distortion. Part II: Oscillations. *J. Atmos. Sci.,* **48,** 2245–2264.

Brandes, E. A., A. V. Ryzhkov, and D. S. Zrnić, 2001: An evaluation of radar rainfall estimates from specific differential phase. *J. Atmos. Oceanic Technol.,* **18,** 363–375.

——, G. Zhang, and J. Vivekanandan, 2002: Experiments in rainfall estimation with a polarimetric radar in a subtropical environment. *J. Appl. Meteor.,* **41,** 674–685.

——, ——, and J. Vivekanandan, 2003: An evaluation of a drop distribution–based polarimetric radar rainfall estimator. *J. Appl. Meteor.,* **42,** 652–660.

Bringi, V. N., V. Chandrasekar, and R. Xiao, 1998: Raindrop axis ratios and size distributions in Florida rainshafts: An assessment of multiparameter radar algorithm. *IEEE Trans. Geosci. Remote Sens.,* **36,** 703–715.

Chandrasekar, V., and V. N. Bringi, 1987: Simulation of radar reflectivity and surface measurements of rainfall. *J. Atmos. Oceanic Technol.,* **4,** 464–478.

——, A. Cooper, and V. N. Bringi, 1988: Axis ratios and oscillations of raindrops. *J. Atmos. Sci.,* **45,** 1323–1333.

Dou, X., W. Liu, P. Amayene, and J. Liu, 1999: Optimization of the parameter of the raindrop size distribution in rain rate measurement by airborne radar. *Quart. J. Appl. Meteor.,* **10,** 293–298.

Doviak, J. D., and D. S. Zrnić, 1993: *Doppler Radar and Weather Observations.* 2d ed. Academic Press, 562 pp.

Gorgucci, E., and G. Scarchilli, 1997: Intercomparison of multiparameter radar algorithms for estimating rainfall rate. Preprints, *28th Conf. on Radar Meteorology,* Austin, TX, Amer. Meteor. Soc., 55–56.

Illingworth, A. J., and T. M. Blackman, 2002: The need to represent raindrop size spectra as normalized gamma distributions for the interpretation of polarization radar observations. *J. Appl. Meteor.,* **41,** 286–297.

——, J. W. F. Goddard, and S. M. Cherry, 1987: Polarization radar studies of precipitation development in convective storms. *Quart. J. Roy. Meteor. Soc.,* **113,** 469–489.

Jameson, A. R., 1983: Microphysical interpretation of multiparameter radar measurements in rain. Part I: Interpretation of polarization measurements and estimation of raindrop shapes. *J. Atmos. Sci.,* **40,** 1792–1802.

Keenan, T. D., L. D. Carey, D. S. Zrnić, and P. T. May, 2001: Sensitivity of 5-cm wavelength polarimetric radar variables to raindrop axial ratio and drop size distribution. *J. Appl. Meteor.,* **40,** 526–545.

Kozu, T., and K. Nakamura, 1991: Rain parameter estimation from dual-radar measurements combining reflectivity profile and path-integrated attenuation. *J. Atmos. Oceanic Technol.,* **8,** 259–270.

Laws, J. O., and D. A. Parsons, 1943: The relationship of raindrop size to intensity. *Trans. Amer. Geophys. Union,* **24,** 452–460.

List, R., 1988: A linear radar reflectivity–rain rate relationship for steady tropical rain. *J. Atmos. Sci.,* **45,** 3564–3572.

Marshall, J. S., and W. Palmer, 1948: The distribution of raindrops with size. *J. Meteor.,* **5,** 165–166.

Oguchi, T., 1983: Electromagnetic wave propagation and scattering in rain and other hydrometeors. *Proc. IEEE,* **71,** 1029–1078.

Pruppacher, H. R., and R. L. Pitter, 1971: A semi-empirical determination of the shape of cloud and rain drops. *J. Atmos. Sci.,* **28,** 86–94.

Rosenfeld, D., and C. W. Ulbrich, 2003: Cloud microphysical properties, processes, and rainfall estimation opportunities. *Radar and Atmospheric Science: A Collection of Essays in Honor of David Atlas,* R. M. Wakimoto and R. Srivastava, Eds., Amer. Meteor. Soc., 237–258.

Ryzhkov, A. V., and D. S. Zrnić, 1995: Comparison of dual-polarization radar estimators of rain. *J. Atmos. Oceanic Technol.,* **12,** 249–256.

——, ——, G. Huang, E. A. Brandes, and J. Vivekanandan, 1999: Characteristics of hydrometer orientation obtained from radar polarimetric measurements in a linear polarization basis. *Proc. IGARSS'99,* Hamburg, Germany, IEEE, 702–704.

Sachidananda, M., and D. S. Zrnić, 1987: Rain rate estimates from differential polarization measurements. *J. Atmos. Oceanic Technol.,* **4,** 588–598.

Seliga, T. A., and V. N. Bringi, 1976: Potential use of radar differential reflectivity measurements at orthogonal polarizations for measuring precipitation. *J. Appl. Meteor.,* **15,** 69–76.

Smith, P. L., 1998: Raindrop size distributions: Exponential or gamma—Does it make a difference? Preprints, *Conf. on Cloud Physics,* Everett, WA, Amer. Meteor. Soc., 399–402.

Testud, J., S. Oury, R. A. Black, P. Amayenc, and X. Dou, 2001: The concept of ''normalized'' distributions to describe raindrop spectra: A tool for cloud physics and cloud remote sensing. *J. Appl. Meteor.,* **40,** 1118–1140.

Tokay, A., and D. A. Short, 1996: Evidence for tropical raindrop spectra of the origin of rain from stratiform versus convective clouds. *J. Appl. Meteor.,* **35,** 355–371.

Ulbrich, C. W., 1983: Natural variations in the analytical form of the raindrop size distribution. *J. Climate Appl. Meteor.,* **22,** 1764–1775.

——, and D. Atlas, 1998: Rain microphysics and radar properties: Analysis methods for drop size spectra. *J. Appl. Meteor.,* **37,** 912–923.

Vivekanandan, J., S. M. Ellis, R. Oye, D. S. Zrnić, A. V. Ryzhkov, and J. Straka, 1999a: Cloud microphysics retrieval using S-band dual-polarization radar measurements. *Bull. Amer. Meteor. Soc.,* **80,** 381–388.

——, G. Zhang, and A. V. Ryzhkov, 1999b: Estimation of canting angle distribution of raindrop spectra using radar measurements. Preprints, *Int. Radar Symp.,* Bangalore, India, IETE and IEEE, 209–218.

——, ——, and M. K. Politovich, 2001: An assessment of droplet size and liquid water content derived from dual-wavelength radar measurements to the application of aircraft icing detection. *J. Atmos. Oceanic Technol.,* **18,** 1787–1798.

——, ——, S. Ellis, D. Rajopadhyayay, and S. Avery, 2003: Radar reflectivity calibration using differential propagation phase measurement. *Radio Sci.,* **38,** 8049, doi:10.1029/2002RS002676.

Williams, C. R., A. Kruger, K. S. Gage, A. Tokay, R. Cifelli, W. F. Krajewski, and C. Kummerow, 2000: Comparison of simultaneous rain drop size distribution estimated from two surface disdrometers and a UHF profiler. *Geophys. Res. Lett.,* **27,** 1763–1766.

Willis, P. T., 1984: Functional fits to some observed drop size distributions and parameterization of rain. *J. Atmos. Sci.,* **41,** 1648–1661.

Yuter, S., and R. A. Houze, 1997: Measurements of raindrop size distributions over the Pacific warm pool and implications for *Z–R* relations. *J. Appl. Meteor.,* **36,** 847–867.

Zhang, G., J. Vivekanandan, and E. Brandes, 2001: A method for estimating rain rate and drop size distribution from polarimetric radar measurements. *IEEE Trans. Geosci. Remote Sens.,* **39,** 830–841.

——, ——, and ——, 2003: The shape–slope relation in observed gamma raindrop size distribution: Statistical error or useful information? *J. Atmos. Oceanic Technol.,* **20,** 1106–1119.